Absorption profile modulation by means of 1D digital plasmonic gratings

P. Zilio,[1,2] D. Sammito,[2,3,4] G. Zacco,[1,2,3] and F. Romanato[1,2,3] *

[1]*Physics Department, Padova University, via Marzolo 8, 35131 Padova, Italy*
[2]*LaNN Laboratory for Nanofabrication of Nanodevices, Corso Stati Uniti 4, 35131 Padova, Italy*
[3]*IOM CNR, TASC Laboratory, via S.S. 14, Km 163.5 in Area Science Park, Basovizza 34012, (TS) Italy*
[4]*Physics Department, Trieste University, Piazzale Europa 1, 34127 Trieste, Italy*
**romanato@tasc.infm.it*

Abstract: Optical simulations of 1D digital plasmonic gratings on a Silicon substrate are performed by means of the Finite Elements Method and a modal analysis. The different mechanisms of transmission of the light are elucidated. The absorption profile in Silicon can be modulated and controlled changing the geometry. Configuration maps allow to determine the different optical regimes. Surface Plasmon Polaritons and cavity-mode resonances are shown to be effectively exploitable to enhance NIR-light absorption in different shallower regions of the underlying Silicon.

OCIS codes: (240.6680) Surface plasmons; (250.5403) Plasmonics; (050.6624) Subwavelength structures.

References and links

1. H. Rather, *Surface Plasmons* (Springer-Verlag, 1988).
2. J. S. White, G. Veronis, Z. Yu, E. S. Barnard, A. Chandran, S. Fan, and M. L. Brongersma, "Extraordinary optical absorption through subwavelength slits," Opt. Lett. **34**(5), 686–688 (2009).
3. D. Derkacs, S. H. Lim, P. Matheu, W. Mar, and E. T. Yu, "Improved performance of amorphous silicon solar cells via scattering from surface plasmon polaritons in nearby metallic nanoparticles," Appl. Phys. Lett. **89**(9), 093103 (2006).
4. S. Pillai, K. R. Catchpole, T. Trupke, and M. A. Green, "Surface Plasmon enhanced silicon solar cells," J. Appl. Phys. **101**(9), 093105 (2007).
5. N. C. Panoiu, and R. M. Osgood, Jr., "Enhanced optical absorption for photovoltaics via excitation of waveguide and plasmon-polariton modes," Opt. Lett. **32**(19), 2825–2827 (2007).
6. R. A. Pala, J. White, E. Barnard, J. Liu, and M. L. Brongersma, "Design of plasmonic thin-film solar cells with broadband absorption enhancements," Adv. Mater. **21**(34), 3504–3509 (2009).
7. D. Crouse, and P. Keshavareddy, "A method for designing electromagnetic resonance enhanced silicon-on-insulator metal-semiconductor-metal photodetectors," J. Opt. A, Pure Appl. Opt. **8**(2), 175–181 (2006).
8. J. A. Shackleford, R. Grote, M. Currie, J. E. Spanier, and B. Nabet, "Integrated plasmonic lens photodetector," Appl. Phys. Lett. **94**(8), 083501 (2009).
9. E. D. Palik, *Handbook of Optical Constants of Solids* (Elsevier, 1998).
10. L. D. Landau, and E. M. Lifshitz, *Electrodynamics of Continuous Media,* (Pergamon, 1984), pp. 272–6.
11. B. Sturman, E. Podivlov, and M. Gorkunov, "Theory of extraordinary light transmission through arrays of subwavelength slits," Phys. Rev. B **77**(7), 075106 (2008).
12. J. A. Porto, F. J. García-Vidal, and J. B. Pendry, "Transmission resonances on metallic gratings with very narrow slits," Phys. Rev. Lett. **83**(14), 2845–2848 (1999).
13. F. J. García-Vidal, and L. Martin-Moreno, "Transmission and focusing of light in one-dimensional periodically nanostructured metals," Phys. Rev. B **66**(15), 155412 (2002).
14. D. Crouse, "Numerical modeling and electromagnetic resonant modes in complex grating structures and optoelectronic device applications," IEEE Trans. Electron. Dev. **52**(11), 2365–2373 (2005).
15. R. Gordon, "Light in a subwavelength slit in a metal: Propagation and reflection," Phys. Rev. B **73**(15), 153405 (2006).
16. F. Medina, F. Mesa, and D. C. Skigin, "Extraordinary optical transmission through arrays of slits: a circuit theory model," IEEE Trans. Microw. Theory Tech. **58**(1), 105–115 (2010).
17. T. W. Ebbesen, H. J. Lezec, H. F. Ghaemi, T. Thio, and P. A. Wolff, "Extraordinary optical transmission through sub-wavelength hole arrays," Nature **391**(6668), 667–669 (1998).
18. H. Liu, and P. Lalanne, "Microscopic theory of the extraordinary optical transmission," Nature **452**(7188), 728–731 (2008).

#126896 - $15.00 USD Received 12 Apr 2010; revised 26 May 2010; accepted 27 May 2010; published 31 Aug 2010

19. J. Weiner, "The physics of light transmission through subwavelength apertures and aperture arrays," Rep. Prog. Phys. **72**(6), 064401 (2009).
20. Q. Cao, and P. Lalanne, "Negative role of surface plasmons in the transmission of metallic gratings with very narrow slits," Phys. Rev. Lett. **88**(5), 057403 (2002).
21. L. Rayleigh, "On the dynamical theory of gratings," Proc. R. Soc. Lond., A Contain. Pap. Math. Phys. Character **79**(532), 399–416 (1907).
22. Y. Xie, A. R. Zakharian, J. V. Moloney, and M. Mansuripur, "Transmission of light through periodic arrays of sub-wavelength slits in metallic hosts," Opt. Express **14**(14), 6400–6413 (2006).
23. Y. Takakura, "Optical resonance in a narrow slit in a thick metallic screen," Phys. Rev. Lett. **86**(24), 5601–5603 (2001).
24. F. Marquier, J. J. Greffet, S. Collin, F. Pardo, and J. L. Pelouard, "Resonant transmission through a metallic film due to coupled modes," Opt. Express **13**(1), 70–76 (2005).

1. Introduction

The peculiar optical properties of metallic nanostructures are finding more and more applications as a mean to tailor the natural characteristics of bulk materials. In particular Surface Plasmons at interfaces between nanostructured metals and dielectrics are known to give the chance to highly enhance the local EM fields [1]. If the dielectric has a non zero absorption coefficient this also results in a strong enhancement of optical absorption [2] with possible applications for efficiency improvement of semiconductor devices such as solar cells or photodetectors. For example, the overall efficiency of Silicon based Solar Cells generally suffers from the low absorption in the NIR part of the spectrum (wavelengths > 900nm). Great efforts have been devoted to study a way to exploit the high scattering cross section of metal nanoparticles and their light trapping properties in Si solar cells [3,4]. Some recent works considered also periodic nanostructures and demonstrated their effectiveness in applications to thin film solar cells [5,6] and Metal-Semiconductor-Metal photodetectors [7,8].

The purpose of this work is to show and clarify with both numerical and analytical simulations how the different optical resonances of 1D digital metallic gratings (Fig. 1) can be exploited to modulate the EM field absorption profile in an underlying bulk substrate. We focus on the optical response of a digital Gold grating on a semi-infinite Silicon substrate to a normally impinging 1000nm-monochromatic wave, varying systematically both thickness (h) and period (d) of the grating. Different geometric configurations can change dramatically the absorption profile, concentrating the EM fields in close proximity of the metallic nanostructure or simply reducing the absorption extinction depth. Configuration maps allow to point out the different regimes whose mechanisms of EM field distribution have been elucidated by a comparison of numerical and analytical models.

2. Finite Elements model setup

The system has been studied using the commercial software COMSOL Multiphysics® which implements the Finite Elements Method (FEM). In order to minimize computational time and to improve precision, the full EM fields distributions have been computed with FEM only in one period of the grating, setting periodic boundary conditions, and within very thin layers of Silicon and vacuum (see Fig. 1). The ratio between slit width and period is kept constant to 0.1. Of course, the asymmetry of the structure between x and y axis, determines different optical responses for different polarizations of the incident light. In this work we consider only TM polarized (i.e. magnetic field parallel to the metal stripes) incident light since it is the only polarization that can give rise to SPPs in an 1D metallic grating. The dielectric constants of Gold and Silicon at 1000nm were taken to be $\varepsilon_m = -46.4 + 3.5i$ and $\varepsilon_3 = 12.9 + 3.6\cdot 10^{-3}i$ respectively [9]. Gold was chosen because of its low dissipation in the NIR compared to other metals and because of its well defined plasmonic properties, since $\left|\varepsilon_m''\right| \ll \left|\varepsilon_m'\right|$ [1].

Far fields have been reconstructed with the following procedure. We performed a 1D Fourier Transform of the FEM-computed fields along x direction at a given depth, and in the k_x-space we filtered out the non z-propagating modes. Far fields were then obtained transforming back in the real space, taking into account absorption in Silicon. For each

#126896 - $15.00 USD Received 12 Apr 2010; revised 26 May 2010; accepted 27 May 2010; published 31 Aug 2010

configuration (*h,d*) we calculated, within different depths in Silicon, transmittance and absorptance (that is the volume integral over the Silicon layer of the quantity $\frac{1}{2}\omega\varepsilon_3''|\mathbf{E}|^2$, being

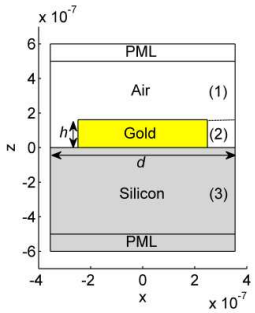

Fig. 1. (Color online) Sketch of the model.

w the angular frequency and **E** the electric field [10]). We also computed the effective absorption profile of light as a function of depth in Silicon (*Q(z)*) averaging the local absorption over one period length of the plasmonic array.

3. Modal analysis of the 1D digital grating

In order to have an insight into the physics of our system an analytic approach is necessary beside the purely numerical one given by FEM. A recent rigorous modal analysis of the system has been performed by Sturman et al. [11]. It considers separately the fields in the regions above and below the grating and within the slits (we indicate them with numbers 1, 3, and 2 respectively, see Fig. 1). Fields in regions 1 and 3 are expanded in loch-Floquet modes while in region 2 they are expanded in the complete set of eigenmodes (propagating, evanescent and anomalous) of the 1D plasmonic crystal given by the alternating metal and dielectric layers. The full field reconstruction is then obtained through field matching at 1-2 and 2-3 interfaces, according to Maxwell's equations. We followed a simplification of this approach [12,13], which nevertheless catches the main physics and has the advantage of leading to simple analytical expressions for the relevant physical quantities (such as transmittance). It is found neglecting, in region 2, all the evanescent modes and keeping only the propagating ones, neglecting losses. If the slit width is smaller than the vacuum wavelength of the incident radiation, only the fundamental propagating eigenmode is allowed. At the horizontal interfaces Surface Impedance Boundary Conditions are imposed [14].

According to this simplified model, the transmittance of the structure results to be

$$T = \frac{1}{\sqrt{\varepsilon_3'}} \frac{|\tau_{12}|^2 \sum_{i=-\infty}^{+\infty} \cos\theta_i \, |\tau_{23,i}^2|^2}{\left|1 - |\rho_{12}||\rho_{23}| e^{i\phi_{tot}}\right|^2}, \tag{1}$$

where t and r are the single-interface (1-2 and 2-3) magnetic field amplitude transmission and reflection coefficients, q_i is the *i*-th diffraction order angle, and f_{tot} is the total phase accumulated by the single propagating waveguide mode travelling back and forth in the slit:

$$\phi_{tot} = \arg(\rho_{12}) + \arg(\rho_{23}) + 2k_0 N_{eff} h, \tag{2}$$

being k_0 the vacuum wave vector. It has been shown [15] that actually the model fails if $|\varepsilon_m|$ is low and/or the slit width is very small with respect to the wavelength of the incident light, since these situations correspond to high penetration of the fields in the metal and the plasmonic contributions to the fields are relevant. In our case of $|\varepsilon_m| \sim 46$, problems arise when the slit width is lower than 10% of the wavelength of incident light. The main deviation from

#126896 - $15.00 USD Received 12 Apr 2010; revised 26 May 2010; accepted 27 May 2010; published 31 Aug 2010

the simple model is found in the propagation constant of the fundamental waveguide propagating mode inside the slits whose effective wave vector results to be higher than the vacuum wave vector. The effect can be taken into account assuming the presence of an effective medium inside the slits with proper refractive index N_{eff}. Following the results found by Sturman et al. [11], we took an effective refractive index $N_{eff} = C/a + 1$, being a the slit width, with an optimal constant C of about 30nm.

Equation (1) allows to identify the main features of the optical response of the 1D plasmonic grating that turn out to be the following:

1) *Cavity mode (CM) resonances*. These resonances result from the multiple scattering of the single propagating mode inside the slits. The mode is partially reflected and transmitted at the slit ends. When the phase difference f_{tot} between the waves transmitted in the substrate is a multiple of 2p, a peak in transmittance is observed, like in a Fabry-Perot resonator. The interesting fact is that, when this resonance takes place, a great fraction of the incident light is channeled within the slits and is transmitted in the substrate (Fig. 2.a). This phenomenon is commonly referred as Extraordinary Optical Transmission (EOT) [11–14,16–20].

2) *Surface Plasmon Polariton (SPP)* resonances. SPPs are surface EM waves which propagate at a metal-dielectric interface and are evanescent in the normal direction (Fig. 2.b). They are excited in a 1D grating when the in-plane component of the incident p-polarized radiation and that one of the scattered waves sum up to match the SPP momentum, i.e.

$$k_0 \sin\alpha + nG = k_0 \,\mathrm{Re}\left(\sqrt{\varepsilon\varepsilon_m / (\varepsilon + \varepsilon_m)}\right) \quad n = 1, 2...$$

with α incidence angle, $G = 2p/d$ and ε the dielectric constant of the facing insulator (vacuum for 1-2 interface, Silicon for 2-3 interface). This kind of resonance is associated to a transmittance extinction and to a high field enhancement in proximity of the grating (hundreds of nm in Silicon) [20].

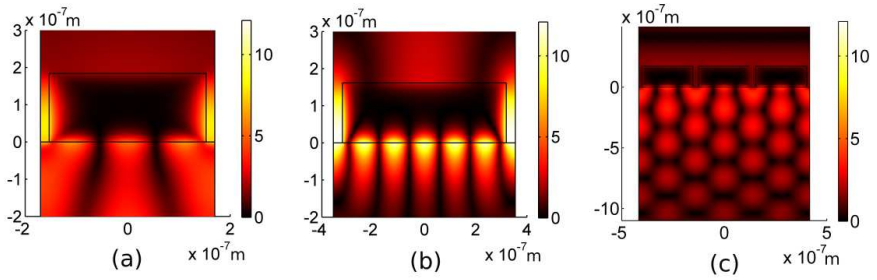

Fig. 2. (Color online) Magnetic field norm enhancements. (a) h = 184nm, d = 340nm: CM-resonance; (b) h = 161nm, d = 710nm: SPP-CM resonance; (c) h = 175nm, d = 278nm: WR-CM resonance.

3) *Wood-Rayleigh anomalies* (WR) [21]. Abrupt changes in transmittance as a function of period are observed in configurations for which a diffraction order lies in the plane of the grating (Fig. 2.c), i.e. at periods $d_n = n\lambda/N$, being N the refractive index of the dielectric medium. These configurations mark a discontinuity since for $d>d_n$ the n-th diffraction order does exist while for $d<d_n$ it does not. It is generally accepted that the peak in transmission is due to the abrupt redistribution of energy among the allowed orders passing through the $d = d_n$ configurations [22]. WR anomalies are not resonant phenomena but rather are due to pure geometrical reasons and are fully independent of CM and SPPs.

#126896 - $15.00 USD Received 12 Apr 2010; revised 26 May 2010; accepted 27 May 2010; published 31 Aug 2010

It is worth noting that CMs are *local* resonances, since they would appear as well in a single illuminated slit without any periodicity [23]. On the other hand SPPs are *global* resonances since they can exist thanks to the coherent periodicity of the structure [1]. As many authors pointed out, however, CMs and SPPs are not independent each other [24]. Actually one should better speak of a hybrid mode which presents both CM and SPP resonant characteristics. The SPP character dominates the transmission properties of the grating as the pitch gets proximate to one of those satisfying Eq. (2). On the other hand the EOT efficiency is greatly enhanced in presence of a periodic structure [21].

4. Results and discussion

In Fig. 3 we report the resulting maps of transmittance and of absorption within 300nm in Silicon obtained with FEM. The values are normalized to the case of purely absorbing Silicon substrate coated with a perfect anti-reflection coating providing unitary transmittance. Resonant (*h,d*) configurations predicted by the semi-analytical model are reported as well (see caption of Fig. 3 for details). The periods chosen for the simulation are smaller than the wavelength of incident light. In the Silicon substrate, however, λ_0/N_{Si} ~ 278nm, so that diffractive effects are present.

Looking at the transmittance map (Fig. 3.a) we see that cavity modes resonances (black lines) are clearly associated with an enhanced transmission in the (*h,d*) configurations far from the SPP resonant ones (grey lines) in which the dominant SPP character determines a transmission extinction. In order to facilitate the resonances identification, in this computation we have chosen a slit-to-period ratio of only 10%. Notwithstanding the small opening fraction, the maximum transmittance value obtained for h = 184nm, d = 340nm is as high as 0.68, reaching the value of bare Silicon. Considerably larger transmittances can be obtained optimizing the duty cycle (for h = 184nm d = 340nm, a maximum transmittance of 0.94 is obtained with a duty cycle of 31%)

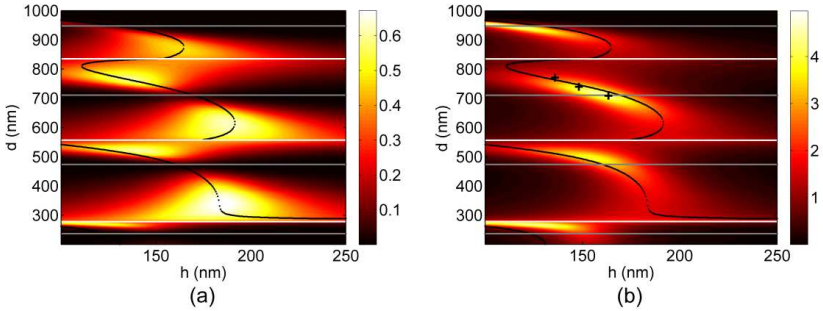

Fig. 3. (Color online) FEM-calculated transmittance (a) and absorption enhancement (b) map within 300nm in Silicon with respect to perfect AR-coated Silicon. Overplotted black and grey lines mark respectively CM and SPP resonances according to the analytical model. White lines mark configurations which present a WR anomaly. Crosses mark configurations whose absorption profile is reported in Fig. 4.a.

Cavity modes are also correlated to absorption enhancements. Within 300nm in Silicon (Fig. 3.b), the largest enhancements (up to 350%) are obtained when both the conditions for SPP and cavity mode excitation are satisfied at the same time (at the crossing between gray black lines). In these configurations CM resonances canalize the whole incident power into an SPP mode rather than into a *z*-propagating mode, giving rise to an extraordinary SPP (Fig. 2.b). By conversion in Fig. 2.a it is shown the typical much weaker field enhancement in a configuration where only CM is excited without SPP resonant coupling. Looking at the absorption profiles (Fig. 4.a) we observe that, in strongly SPP-CM-resonant configurations (black line), most of the enhancement is confined in the metal proximity and decays

#126896 - $15.00 USD Received 12 Apr 2010; revised 26 May 2010; accepted 27 May 2010; published 31 Aug 2010

exponentially within the typical plasmonic decay length [1] $L \approx (\lambda / 2\pi) \cdot [(|\varepsilon_m'| + \varepsilon_3') / \varepsilon_3'^2]^{1/2}$ ~100nm. The enhancement factor can be up to 30 times in the first 30nm of Silicon.

Far from the grating (Fig. 4.a, inset) the absorption is almost zero in SPP resonances since SPPs typically produce transmission extinctions. On the other hand, strong CM but not SPP resonant configurations (light grey lines) show absorption profiles that are much less confined close to the surface, but are higher in depth due to EOT.

Looking at the absorption within a thicker (40μm) Silicon layer (Fig. 5.a) we find that the best enhancements are obtained in CM-resonant configurations proximate to WR anomalies, i.e. those shown in Fig. 2.c. In these configurations, CM resonance results to efficiently couple to diffracted waves propagating at grazing angles with respect to the grating plane. The

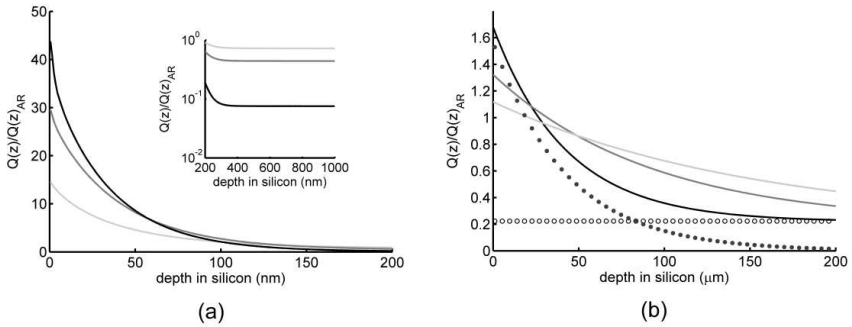

Fig. 4. (a) Absorption profile enhancement with respect to perfect AR-coated Silicon in configurations marked with crosses in Fig. 3: h = 136nm,d = 765nm (light gray); h = 148nm,d = 735 (medium gray); h = 163nm, d = 705nm (black); inset: absorption profiles within 1μm depth. (b) Absorption profile enhancement in configurations near the cross in Fig. 5: *h* = 175nm and *d* respectively 285nm (black), 300nm (medium gray), 320nm (light gray). Black dots and circles represent the contributions to the whole black absorption profile coming from the $n = \pm 1$ and n = 0 diffraction orders respectively.

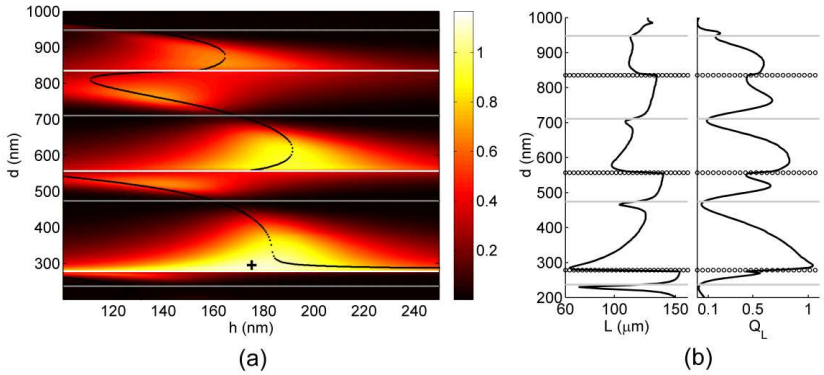

Fig. 5. (color online) (a) Absorption enhancement within 40μm in Silicon with respect to Silicon treated with perfect AR coating. Overplotted lines are defined as in Fig. 3. (b) Left: Extinction length of the absorption profiles calculated in CM-resonant configurations ($h_{CM}(d),d$); right: absorption within *L* with grating normalized to absorption within the same *L* in case of perfect AR-coated Silicon. Grey horizontal lines and circles mark respectively SPP-resonant periods and WR anomalies.

mechanism is particularly efficient when only the $n = \pm 1$ diffraction orders are present besides the 0-th one, around configuration identified with a black cross in Fig. 5.a (*h* = 175nm, *d* = 290nm). Looking at the absorption profiles (Fig. 4.b), these are clearly the superposition of two exponential decays, relative to the $n = \pm 1$ and *n* = 0 diffraction orders respectively. As can be seen, in high enhancement configurations, the $n = \pm 1$ orders

#126896 - $15.00 USD Received 12 Apr 2010; revised 26 May 2010; accepted 27 May 2010; published 31 Aug 2010

contribute significantly to the whole absorption profile (see dotted lines in Fig. 4.b) which remains higher than that of a perfect AR-coated Silicon up to about 40μm depth.

The strong absorption enhancement in proximity of the grating in presence of SPP resonances is also correlated to an high power dissipation in metal. The *h*-*d* map of absorptance in metal looks very similar to Fig. 3.b and we do not report it. The maximum absorptance of metal reaches values up to 84% (*h* = 163nm, *d* = 765nm) in correspondence of SPP-CM resonant configurations, down to about 14% (*h* = 175nm, *d* = 285nm) near CM-WR configurations.

In order to highlight the strong field confinement achievable with CM-WR coupling, we consider now the locus of CM-resonant configurations, i.e., for every period *d*, we consider the thickness $h_{CM}(d)$ which maximizes the FEM-calculated transmittance. In these configurations we consider an absorption profile extinction length (*L*) taking the depth in Silicon at which a fraction of $(1\text{-}e^{-1})$ ~63.2% of the transmitted power is absorbed. This is the fraction of power absorbed within the typical decay length in presence of an exponential-like absorption profile. We finally calculate the absorption enhancement within *L* ($^{\circ}Q_L$) integrating *Q(z)* down to depth *L* and normalizing point by point to the absorption within *L* with respect to the case of a perfect AR-coated film on Silicon. In Fig. 5.b we report *L* and Q_L as a function of period, being $h = h_{CM}(d)$. It is clearly seen that at CM-resonant configurations just above WR anomalies the extinction length drops while the absorption within *L* is strongly increased. Although most of the Q_L are lower than 1, it is to be noted that we have an extraordinary absorption for every period at which Q_L exceeds 0.1, i.e. the fraction of period not covered by metal. As a general comment it clearly appears that the absorption length is always much shorter than the corresponding for pure absorption in Silicon (156μm at 1000nm wavelength) and almost always accompanied by an enhancement of absorption with respect to the normalized open area.

The absorption enhancement can be greatly improved optimizing the duty cycle. In Fig. 6 we show the trends of *L* and Q_L as a function of the duty cycle for the fixed (*h*,*d*)-configuration *h* = 145nm, *d* = 280nm, which is very close to the WR-anomaly (see Fig. 5.a). The maximum of absorption is found 1.5 times greater than in AR-coated silicon within *L* = 80μm

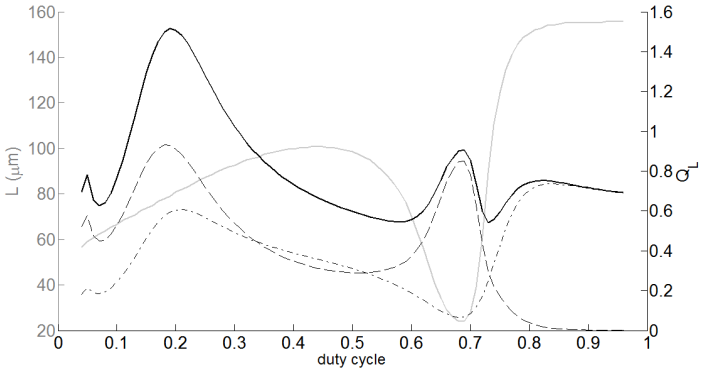

Fig. 6. Gray: Extinction length of the absorption profile for different duty cycle values; black: absorption within *L* normalized to absorption within the same *L* in case of perfect AR-coated Silicon. Dash-dotted and dashed lines are the contribution to Q_L from the n = 0 and n = ± 1 diffraction orders respectively. *h* and *d* are set to 145nm and 280nm respectively. The set of parameters h = 145, d = 280, duty cycle = 0.2 was found to optimize the absorption enhancement within 40μm (+ 210%).

for a duty cycle of about 20%. As can be seen, in this configuration most of the power transmitted by the CM in the slit is drained by the n = ± 1 diffracted waves. We note that the extinction length drops at a duty cycle of about 0.7, before reaching the value it has in absence

#126896 - $15.00 USD Received 12 Apr 2010; revised 26 May 2010; accepted 27 May 2010; published 31 Aug 2010

of grating, while Q_L has a local maximum. This is due to a stronger coupling of the CM-resonances to the $n = \pm 1$ diffraction orders than to the $n = 0$.

5. Conclusions

Summarizing, we studied the optical response of 1D digital plasmonic gratings placed on a semi-infinite absorbing substrate in order to clarify the role and the potentialities that the optical resonances of such structures have in remodulating light absorption.

Numerical and analytical simulations show that relevant absorption enhancements can be produced in Silicon at different depths, in relation to the type of plasmonic resonance involved. SPPs resonances lead to high field enhancement (up to + 350%) in close proximity to the grating, whereas cavity modes coupled to grazing diffracted waves allow an efficient transmission and spreading of light power into the substrate, leading to an enhanced absorption of long-wavelength radiation in shallower regions of the underlying Silicon (up to + 51.3% within 80μm). The results may be useful to design high efficiency Silicon-based photodetectors devices active in the IR spectral range. Further studies will be addressed to the wavelength response of the gratings in order to obtain absorption enhancement over wide bandwidth with possible applications in solar cells.

Acknowledgments

The authors gratefully acknowledge support from project ORION of European Community, grant agreement 222517. In particular, Da. Sammito thanks ORION project for the research grant.

#126896 - $15.00 USD Received 12 Apr 2010; revised 26 May 2010; accepted 27 May 2010; published 31 Aug 2010